Meissner currents induced by topological magnetic textures in hybrid superconductor/ferromagnet structures

Samme M. Dahir, Anatoly F. Volkov, and Ilya M. Eremin

Institut für Theoretische Physik III, Ruhr-Universität Bochum, D-44780 Bochum, Germany

Topological spin configurations in proximity to a superconductor have recently attracted great interest due to the potential application of the former in spintronics and also as another platform for realizing nontrivial topological superconductors. Their application in these areas requires precise knowledge of the existing exchange fields and/or the stray fields, which are therefore essential for the study of these systems. Here, we determine the effective stray field $\mathbf{H}_{str}$ and the Meissner currents $\mathbf{j}_S$ in a superconductor/ferromagnet/superconductor (S/F/S) junction produced by various nonhomogenous magnetic textures $\mathbf{M}(\mathbf{r})$ in the F. The inhomogeneity arises either due to a periodic structure with flat domain walls (DW) or is caused by an isolated chiral magnetic skyrmion (Sk). We consider both Bloch- and Néel-type Sk and also analyze in detail the periodic structures of different types of DW's, that is, Bloch-type DW (BDW) and Néel-type DW (NDW) of finite width with in- and out-of-plane magnetization vector $\mathbf{M}(x)$. The spatial dependence of the fields $\mathbf{H}_{str}(\mathbf{r})$ and Meissner currents $\mathbf{j}_S(\mathbf{r})$ are shown to be qualitatively different for the case of Bloch- and Néel-type magnetic textures. While the spatial distributions in the upper and lower S are identical for Bloch-type Sk and DW's they are asymmetric for the case of Néel-type magnetic textures. The depairing factor, which determines the critical temperature T_c and which is related to the vector potential of the stray field, can have its maximum at the center of a magnetic domain but also, as we show, above the DW. For Sk's, the maximum is located at a finite distance within the Sk radius r_{Sk}. Based on this, we study the nucleation of superconductivity in the presence of DW's. Because of the asymmetry for Néel-type structures, the critical temperature T_c in the upper and lower S is expected to be different. The obtained results can also be applied to S/F bilayers.

I. INTRODUCTION

Over the past decades, continuous efforts have been made to study superconductor-ferromagnet heterostructures due to a variety of interesting features caused by the proximity effect, i.e., the penetration of Cooper pairs from the superconductor (S) into the ferromagnet (F). The most interesting and well established effects are the sign reversal of the Josephson current in S/F/S junctions and the appearance of a long-ranged triplet component (see review articles [1–7] and references therein).

Other interesting features involve the interplay of various types of topological defects that, under certain conditions, can be present in the superconductor and/or ferromagnet. One of these topological defects are the Abrikosov vortices which occur in type-II superconductors [8] in the magnetic field interval, $H_{c1} < H_{ext} < H_{c2}$. There are also several different topological structures that can be found in ferromagnets. The most prominent ones are magnetic domain walls (DW), where the magnetization vector $\mathbf{M}$ rotates by an angle π across the DW. Another example of a topological defect that has received much attention recently due to its potential application in spintronics are the so-called magnetic skyrmions (Sk) [9–12]. These local whirl-like structures are topologically equivalent to two DW's as one can map the inner part of the Sk on the stripes between two domains via conformal transformation. Similar to flat DW's, where the magnetization vector $\mathbf{M}$ changes its direction by rotating either in the (x, z) plane

(Néel type) or in the (y, z) plane (Bloch type), the winding of chiral Sk can either have a Bloch- or a Néel-like structure. Which type of chiral Sk is realized depends on the underlying chiral interaction. Note that there is already some work on the mutual interaction between topological defects occurring in ferromagnets and superconductors, see review [13] and references therein. In the absence of the direct proximity effect (no direct contact between S and F), this interaction is realized through the magnetic stray field $\mathbf{H}_{str}$ generated by the nonuniform magnetic textures in the F and the magnetic field associated with the superconducting vortices. The creation of Pearl and Abrikosov vortices in S/F structures with and without DW's has been analyzed in Refs. [13–17]. More recently, the spontaneous creation of vortices in S/F structures with Sk's with and without direct proximity effect was also studied theoretically [18–23]

As it is well known, there is no stray field $\mathbf{H}_{str}$ outside of uniformly magnetized infinite film [24]. However, within the ferromagnet the magnetic induction $\mathbf{B}^{(F)}$ or the magnetic field $\mathbf{H}^{(F)}$ can still acquire finite values, i.e., $\mathbf{B}^{(F)} = 4\pi\mathbf{M}_0$ and $\mathbf{H}^{(F)} = 0$ for the in-plane magnetization and $\mathbf{B}^{(F)} = 0$ and $\mathbf{H}^{(F)} = -4\pi\mathbf{M}_0$ for the out-of-plane magnetization. Therefore for a uniform magnetization $\mathbf{M}_0$ in the F of a S/F/S structure, both the $\mathbf{B}^{(S)}$, the $\mathbf{H}^{(S)}$ and the Meissner current $\mathbf{j}_S$ are equal zero in the superconductors where $\mathbf{B}^{(S)} = \mathbf{H}^{(S)}$. Thus nonzero stray fields and Meissner currents can only occur if the magnetization of an infinite F is nonhomogeneous. This

was studied in S/F structures with DW's of zero width in Refs. [17,25,26], for DW's of finite width in Ref. [27] and for a magnetic vortex configuration in Ref. [28]. In the presence of a proximity effect and spin-orbit coupling, the Meissner current was recently calculated in a bilayer S/F structure with a particular Néel-type Sk in the F and a vortex in the S [19].

Despite of existing literature, there are still no systematic studies of Meissner currents in S/F and S/F/S structures with different topological magnetic textures (Sk's or flat DW's) with different orientations of the magnetization vector **M**. This is particular interesting due to potential realization of Majorana fermions in such heterostructures [22,29,30]. In the present paper, we address this topic, by analyzing S/F/S systems with an isolated magnetic Sk (Bloch- and Néel-type Sk) or with a periodic flat DW structure (out-of-plane and in-plane magnetization, Bloch and Néel DW's) in the ferromagnetic material.

Assuming that there is no proximity effect present and that there are no Abrikosov vortices in the S/F/S structure, i.e., magnetic stray fields are supposed to be less than the critical field H_{c1}, we find the effective magnetic stray field from which we deduce the induced screening currents $\mathbf{j}_S$. Note that the obtained spatial distribution of the current density $\mathbf{j}_S$ in the S in a Josephson system S/F/S is qualitatively similar to that in S/F bilayer. The knowledge of the effective stray field $\mathbf{H}_{str}$ and the current density $\mathbf{j}_S$ allows one to estimate the region where superconductivity nucleates upon decreasing the temperature T below T_c: either at the DW's or in the center of the domains. Available experimental data point out that the nucleation of superconductivity preferably occurs at the DW's [31]. However, it will be shown that the exact location depends on the considered type of DW's. In addition, we show that new interesting and nontrivial features arise in the system under consideration. For example, we find an pronounced asymmetry in the z dependence of $\mathbf{j}_S(z)$, which occurs for both Néel DW's and Néel-type magnetic Sk's. This asymmetry is characterized by the in-plane dependence $\mathbf{r}_\perp$ of the Meissner current $\mathbf{j}_S(\mathbf{r}_\perp)$ and stray field $\mathbf{H}_{str}(\mathbf{r}_\perp)$, which differs greatly above and below the ferromagnet and can even result in a local sign change of the Meissner current. In the absence of a superconductor, the asymmetry of the stray field for DW's is already known [32]. For instance, it was recently demonstrated in experiments on artificial magnetic structures [33]. The asymmetry arises due to a nonzero $\nabla \cdot \mathbf{M}$ term inside the ferromagnet. In the case of Bloch DW's, such an asymmetry does not appear, since $\nabla \cdot \mathbf{M}$ term vanishes.

This difference between Bloch- or Néel-type DW's and Sk's follows from the different orientation of the vector $\hat{\mathbf{e}}_{rot}$ which describes the rotation axis of the magnetization **M** along the domain wall. For instance, in the case of Bloch- and Néel-type DW one can define a vector $\hat{\mathbf{e}}_N \equiv (\hat{\mathbf{e}}_{rot} \times \hat{\mathbf{e}}_x)$, where $\hat{\mathbf{e}}_x$ is a unit vector normal to the plane of the DW. For Néel-type DW's this vector is nonzero, while for Bloch-type DW's the vector product is zero because the rotation vector $\hat{\mathbf{e}}_{rot}$ is collinear to the vector $\hat{\mathbf{e}}_x$. In the language of magnetic monopoles, which can be used for magnetic stray fields, the presence of $\hat{\mathbf{e}}_N$ translates into the existence of magnetic bulk charges. In combination with the magnetic surface charges, the stray field components of the bulk charges results in the aforementioned asymmetry. In the case of a S/F bilayer it

generally makes no sense to speak about an asymmetry, but the spatial distribution of the Meissner $\mathbf{j}_S$ in the S still depends on the direction of the vector $\hat{\mathbf{e}}_N$ with respect to the F film (upward or downwards).

We will begin this paper by calculating a general expression for the effective magnetic stray field $\mathbf{H}(\mathbf{r})$ in an S/F/S structure generated by a nonhomogeneous two-component magnetization **M**, see Sec. II. From the stray field, we extract an expression for the Meissner current in the two superconducting region, which is then applied to describe induced currents in the presence of isolated Néel- and Bloch-type Sk, see Sec. III, as well as for various magnetic DW configurations, see Sec. IV. In Sec. V, we use a Ginzburg-Landau model in the absence of external currents to estimate the nucleation of superconductivity in the presence of the DW structures, we considered earlier. Note that the obtained results in this sections are independent of the type of S, as we are working with unscreened magnetic stray fields. The universal expressions for these unscreened fields can be easily extracted from our results in the previous section. We end this work with a conclusion in Sec. VI.

II. STRAY FIELD AND MEISSNER CURRENT

We consider an S/F/S structure, that is, a ferromagnetic film of thickness $2d_F$ interfaced by two superconductors at $z = \pm d_F$. The magnetization $\mathbf{M}(\mathbf{r})$ inside the ferromagnet can be written in the form

$$\mathbf{M}(\mathbf{r}) = M_0 \mathbf{n}(\mathbf{r}) \qquad (1)$$

where the unit vector $\mathbf{n}(\mathbf{r})$ is a function of the position vector $\mathbf{r} = (\mathbf{r}_\perp, z)$ with $\mathbf{r}_\perp$ lying in the (x, y) plane. In the following the magnetization is assumed to be independent of the z coordinate.

We will now begin with determining the spatial distribution of the screened stray field in the superconducting regions. The superconducting order parameters (OP) are assumed to be homogeneous. Any magnetic field $\mathbf{H}^{(S)}(\mathbf{r}) = (\mathbf{H}_\perp^{(S)}(\mathbf{r}), \mathbf{H}_z^{(S)}(\mathbf{r}))$ inside the S must then satisfy the London equation which we write for the Fourier component $\mathbf{H}^{(S)}(\mathbf{k}, z) = \int d\mathbf{r}_\perp \mathbf{H}^{(S)}(\mathbf{r}_\perp, z) \exp(-i\mathbf{k} \cdot \mathbf{r}_\perp)$

$$\partial_{zz}^2 \mathbf{H}^{(S)}(\mathbf{k}, z) - \kappa^2 \mathbf{H}^{(S)}(\mathbf{k}, z) = 0, \quad \text{S regions} \qquad (2)$$

where $\kappa^2 = |k|^2 + \lambda_L^{-2}$ and λ_L is the London penetration depth. In the general case, the two superconductors may have different London penetration depth λ_L^+ and λ_L^-. The solution of Eq. (2) is given by

$$\mathbf{H}^{(S)}(\mathbf{k}, z) = \mathbf{C}_\pm(\mathbf{k}) e^{-\kappa_\pm |z|}, \quad \text{S regions} \qquad (3)$$

where the index $\pm$ of the constant $\mathbf{C}_\pm = (\mathbf{C}_\pm^\perp, \mathbf{C}_\pm^z)$ and $\kappa^\pm$ indicates their values in the upper/lower superconducting regions, respectively.

The stray field generated by the magnetization **M** inside the F has to fulfill the magnetostatic condition $\nabla \times \mathbf{H}^{(F)} = 0$ which allows us to define a magnetic scalar potential U with

$$\mathbf{H}^{(F)}(\mathbf{k}, z) = -(i\mathbf{k} U(\mathbf{k}, z), \partial_z U(\mathbf{k}, z)). \qquad (4)$$

In the absence of the proximity effect (PE), the potential U is related to the magnetization **M** via $\nabla \cdot \mathbf{H}^{(F)} = -4\pi \nabla \cdot \mathbf{M}$ so

that we can write

$$\partial_{zz}^2 U(\mathbf{k}, z) - |k|^2 U(\mathbf{k}, z) = 4\pi M_0 i\mathbf{k} \cdot \mathbf{n}_\perp(\mathbf{k}), \quad \text{F film.} \tag{5}$$

Solving Eq. (5) for $U(\mathbf{k}, z)$, we obtain

$$U(\mathbf{k}, z) = 4\pi M_0 \Big\{ A(\mathbf{k}) \sinh(|k|z) + B(\mathbf{k}) \cosh(|k|z) $$
$$- \frac{i\mathbf{k} \cdot \mathbf{n}_\perp(\mathbf{k})}{|k|^2} + C_0\delta(\mathbf{k}) + \frac{i\mathbf{k} \cdot \mathbf{C}_{\mathbf{r}_\perp}}{|k|^2}\delta(\mathbf{k}) \Big\} \tag{6}$$

with the Dirac δ function $\delta(\mathbf{k})$. The last two terms are contributions to the homogeneous solutions of Eq. (5). In the coordinate representation it has the form: $C_0 + \mathbf{C}_\perp \mathbf{r}_\perp$ Note, the constant C_0 does not affect any physical quantity, so that we can set $C_0 = 0$. The constant $\mathbf{C}_\perp$ on the other hand, is related to a noncompensated magnetic moment $\mathbf{M}_{un}$ in the F which turns to zero for $\mathbf{M}_{un} = 0$. Using Eq. (4) we can determine the stray field $\mathbf{H}^{(F)}$ in the F film

$$\mathbf{H}_\perp^{(F)}(\mathbf{k}, z) = -4\pi M_0 i\mathbf{k} \Big\{ A(\mathbf{k}) \sinh(|k|z) $$
$$+ B(\mathbf{k}) \cosh(|k|z) - \frac{i\mathbf{k} \cdot \bar{\mathbf{n}}_\perp(\mathbf{k})}{|k|^2} \Big\}, \tag{7}$$

$$H_z^{(F)}(\mathbf{k}, z) = -4\pi M_0 |k|\{A(\mathbf{k}) \cosh(|k|z) + B(\mathbf{k}) \sinh(|k|z)\}, \tag{8}$$

where we defined

$$\bar{\mathbf{n}}_\perp(\mathbf{k}) := (\mathbf{n}_\perp(\mathbf{k}) - \mathbf{C}_{\mathbf{r}_\perp}\delta(\mathbf{k})). \tag{9}$$

The constants $A(\mathbf{k})$, $B(\mathbf{k})$ and $\mathbf{C}_\pm(\mathbf{k})$ can be found using the matching conditions for the magnetic field and the magnetic

induction at the S/F interfaces. They are reduced to the continuity of the tangential components of the in-plane field $\mathbf{H}_\perp(\mathbf{k}, z)$ and the normal component of the magnetic induction $B_z(\mathbf{k}, z) = H_z(\mathbf{k}, z) + 4\pi M_0 n_z(\mathbf{k})$, i.e.,

$$\mathbf{H}_\perp^{(S)}(\pm d_F) = \mathbf{H}_\perp^{(F)}(\pm d_F), \tag{10}$$

$$H_z^{(S)}(\pm d_F) = H_z^{(F)}(\pm d_F) + 4\pi M_0 n_z(\mathbf{k}). \tag{11}$$

In addition, the in-plane component of $\mathbf{H}^{(S)}$ is coupled to the normal component via the equation $\nabla \cdot \mathbf{H}^{(S)} = 0$ so that

$$\mathbf{C}_\pm^\perp(\mathbf{k}) = \mp \frac{i\mathbf{k}}{|k|} \frac{\kappa_\pm}{|k|} C_\pm^z(\mathbf{k}). \tag{12}$$

Using Eqs. (10)–(12), we can determine the coefficients $A(\mathbf{k})$ and $B(\mathbf{k})$, which are given by

$$A(\mathbf{k}) = n_z(\mathbf{k}) \frac{\kappa_+ D_2^-(k) + \kappa_- D_2^+(k)}{|k| D(k)}$$
$$+ \bar{\mathbf{n}}_\perp(\mathbf{k}) \frac{i\mathbf{k}}{|k|} \frac{D_2^-(k) - D_2^+(k)}{D(k)}, \tag{13}$$

$$B(\mathbf{k}) = n_z(\mathbf{k}) \frac{\kappa_+ D_1^-(k) - \kappa_- D_1^+(k)}{|k| D(k)}$$
$$+ \bar{\mathbf{n}}_\perp(\mathbf{k}) \frac{i\mathbf{k}}{|k|} \frac{D_1^-(k) + D_1^+(k)}{D(k)} \tag{14}$$

with $D(k) = D_1^-(k)D_2^+(k) + D_1^+(k)D_2^-(k)$, where

$$D_1^\pm(k) = |k| \sinh(|k|d_F) + \kappa_\pm \cosh(|k|d_F), \tag{15}$$

$$D_2^\pm(k) = |k| \cosh(|k|d_F) + \kappa_\pm \sinh(|k|d_F). \tag{16}$$

The coefficient $\mathbf{C}_\pm(\mathbf{k})$ is given by

$$C_\pm^z(k) = -4\pi M_0 |k| \sinh(|k|d_F)e^{\kappa_\pm d_F}\Big[\pm\frac{i\mathbf{k}}{|k|} \frac{\bar{\mathbf{n}}_\perp(\mathbf{k})}{D(k)}(\{D_1^-(k) + D_1^+(k)\} \pm \{\kappa_- - \kappa_+\} \cosh(|k|d_F))$$
$$- \frac{n_z(\mathbf{k})}{D(k)}(\{D_2^-(k) + D_2^+(k)\} \pm \{\kappa_- - \kappa_+\} \sinh(|k|d_F))\Big]. \tag{17}$$

For the sake of simplicity, we will from now on consider two identical superconducting materials, i.e., $\lambda_L^+ = \lambda_L^-$. In this case the expression for the coefficients can be reduced to

$$A(\mathbf{k}) = \frac{\kappa}{|k|} \frac{n_z(\mathbf{k})}{D_1(k)}, \quad B(\mathbf{k}) = \frac{i\mathbf{k}}{|k|} \frac{\bar{\mathbf{n}}_\perp(\mathbf{k})}{D_2(k)}, \tag{18}$$

and

$$C_\pm^z(\mathbf{k}) = -4\pi M_0 |k| \sinh(|k|d_F)e^{\kappa d_F}\Big[\pm\frac{i\mathbf{k}}{|k|} \frac{\bar{\mathbf{n}}_\perp(\mathbf{k})}{D_2(k)} - \frac{n_z(\mathbf{k})}{D_1(k)} \Big]. \tag{19}$$

With this we obtain the k-space representation of the screened stray field in an S/F/S junction for two identical superconductors.

In the S region $|z| > d_F$,

$$\tilde{\mathbf{H}}_\perp^{(S)}(\mathbf{k}, z) = \kappa \sinh(|k|d_F)\frac{i\mathbf{k}}{|k|}\Big[\frac{i\mathbf{k}}{|k|} \frac{\bar{\mathbf{n}}_\perp(\mathbf{k})}{D_2(k)} \mp \frac{n_z(\mathbf{k})}{D_1(k)} \Big]e^{-\kappa|z\mp d_F|}, \tag{20}$$

$$\tilde{H}_z^{(S)}(\mathbf{k}, z) = -|k| \sinh(|k|d_F)\Big[\pm\frac{i\mathbf{k}}{|k|} \frac{\bar{\mathbf{n}}_\perp(\mathbf{k})}{D_2(k)} - \frac{n_z(\mathbf{k})}{D_1(k)} \Big]e^{-\kappa|z\mp d_F|}. \tag{21}$$

In the F film $|z| < d_F$,

$$\tilde{\mathbf{H}}_\perp^{(F)}(\mathbf{k}, z) = -\frac{i\mathbf{k}}{|k|}\Big[\frac{i\mathbf{k}}{|k|} \bar{\mathbf{n}}_\perp(\mathbf{k})\Big(\frac{|k| \cosh(|k|z)}{D_2(k)} - 1 \Big)$$
$$+ \frac{n_z(\mathbf{k})\kappa \sinh(|k|z)}{D_1(k)} \Big], \tag{22}$$

$$\tilde{H}_z^{(F)}(\mathbf{k}, z) = -\Big[\frac{i\mathbf{k}}{|k|} \frac{\bar{\mathbf{n}}_\perp(\mathbf{k})|k| \sinh(|k|z)}{D_2(k)} + \frac{n_z(\mathbf{k})\kappa \cosh(|k|z)}{D_1(k)} \Big], \tag{23}$$

where we expressed the results in terms of a dimensionless field $\tilde{\mathbf{H}} = \mathbf{H}/4\pi M_0$.

The obtained expressions describe the screened stray field in an S/F/S structure. By taking $\lambda_L \to \infty$, i.e., $\kappa \to k$, we

can also extract the unscreened stray field which would be present in the absence of superconductors. In this limit, the result describes the general distribution of the stray field created by a nonhomogeneous magnetization in a F in vacuum. The associated vector potential is later used to estimate the nucleation of superconductivity. The origin of the screening field that leads to the effective stray field in Eqs. (22) and (23), are the induced supercurrents inside the S. The supercurrent (Meissner current) $\mathbf{j}_S$ can be determined using Ampère's law $\nabla \times \mathbf{H} = \frac{4\pi}{c}\mathbf{j}_S$.

$$\mathbf{j}_S(\mathbf{r}_\perp, z) = \frac{c}{4\pi}[(\nabla_{\mathbf{r}_\perp} + \hat{\mathbf{e}}_z \partial_z) \times (\mathbf{H}_\perp(\mathbf{r}_\perp, z) + \hat{\mathbf{e}}_z H_z(\mathbf{r}_\perp, z))].$$
$$(24)$$

In the Fourier representation, we further obtain

$$\mathbf{j}_S(\mathbf{k}, z) = \frac{c}{4\pi}[(i\mathbf{k} + \hat{\mathbf{e}}_z \partial_z) \times (\mathbf{H}_\perp(\mathbf{k}, z) + \hat{\mathbf{e}}_z H_z(\mathbf{k}, z))].$$
$$(25)$$

It can easily be shown, that the supercurrent disappears within the F, which is the expected result when the PE is absent. Outside the ferromagnet $|z| > d_F$, we obtain the following expression:

$$\mathbf{j}_S(\mathbf{k}, z) = \frac{cM_0\lambda_L^{-2}}{|k|}\left(\hat{\mathbf{e}}_z \times \frac{i\mathbf{k}}{|k|}\right)\tilde{H}_z^{(S)}(\mathbf{k}, z) \qquad (26)$$

from which we can directly derive the vector potential $\mathbf{A}$ in the superconductor using $\mathbf{j}_S = -c\lambda_L^{-2}\mathbf{A}^{(S)}/4\pi$

$$\mathbf{A}^{(S)}(\mathbf{k}, z) = -\frac{4\pi M_0}{|k|}\left(\hat{\mathbf{e}}_z \times \frac{i\mathbf{k}}{|k|}\right)\tilde{H}_z^{(S)}(\mathbf{k}, z). \qquad (27)$$

III. ISOLATED SKYRMION

In this section, we will set the magnetization profile $\mathbf{M}$ to describe an isolated magnetic skyrmion (Sk) in a ferromagnetic background. It is assumed that the Sk's are stabilized by an underlying chiral interaction resulting in either Bloch- or Néel-type Sk's. The magnetization profile has a cylindrical symmetry and varies along the radial direction ρ so that $\mathbf{r}_\perp = \rho$. The unit vector $\mathbf{n}$ of a chiral Bloch or Néel Sk can then be written as

$$\mathbf{n}_\perp(\rho) = \frac{\rho}{\rho}\sin(\theta(\rho))\Theta(r_{Sk} - \rho), \quad \text{Néel Sk}, \qquad (28)$$

$$\mathbf{n}_\perp(\rho) = \frac{\hat{\mathbf{e}}_z \times \rho}{\rho}\sin(\theta(\rho))\Theta(r_{Sk} - \rho), \quad \text{Bloch Sk}, \qquad (29)$$

for the in-plane component and

$$n_z(\rho) = [1 + \cos(\theta(\rho))]\Theta(r_{Sk} - \rho) - 1, \quad \text{Bloch and Néel Sk} \qquad (30)$$

for the out-of-plane component. Here, $\theta(\rho)$ describes the angular variation of the magnetization with respect to the z axis and $\Theta(r_{Sk} - \rho)$ is a Heaviside step function with r_{Sk} being the skyrmion radius. The Fourier components of $\mathbf{n}(\rho)$ are equal to

$$\mathbf{n}_\perp(\mathbf{k}) = -2\pi\frac{i\mathbf{k}}{k}m_\perp(k), \quad \text{Néel Sk}, \qquad (31)$$

$$\mathbf{n}_\perp(\mathbf{k}) = -2\pi\frac{\hat{\mathbf{e}}_z \times \mathbf{k}}{k}m_\perp(k), \quad \text{Bloch Sk}, \qquad (32)$$

and

$$n_z(\mathbf{k}) = 2\pi[m_z(k) - 2\pi\delta(\mathbf{k})], \quad \text{Bloch and Néel Sk}. \qquad (33)$$

The functions $m_\perp(k)$ and $m_z(k)$ are defined as

$$m_\perp(k) = \int_0^{r_{Sk}} d\rho\rho J_1(k\rho)\sin(\theta(\rho)), \qquad (34)$$

$$m_z(k) = \int_0^{r_{Sk}} d\rho\rho J_0(k\rho)[1 + \cos(\theta(\rho))], \qquad (35)$$

where $J_n(x)$ is the Bessel-function of the first kind of order n. The angular dependence of the Sk profile $\theta(\rho)$, is described using a circular 360°-domain wall ansatz [34].

$$\theta(\rho) = \sum_\pm \arcsin\left[\tanh\left(-\frac{\rho \mp c}{w/2}\right)\right] \qquad (36)$$

with c being the size of the domain core and w is the domain wall width. For the remainder of this work, we set $c = 0$ nm. Using Eq. (36), one can estimate the radius r_{Sk} of the Sk. It should be noted that the expressions in this section can be used for any radially symmetric magnetization profile.

Using the obtained result from the previous section, we will begin analyzing the effective stray field generated by a Sk in our S/F/S structure in the case of two identical superconductors. Afterwards we will determine the corresponding induced Meissner currents. Taking into account that for a Bloch Sk $\mathbf{n}_\perp \propto (\hat{\mathbf{e}}_z \times \mathbf{k})$ [see Eq. (29)], we see that the first term in Eqs. (20)–(23) vanishes. This means that the individual components of the stray field are either symmetric $H_z(z) = H_z(-z)$ or antisymmetric functions $\mathbf{H}_\perp(z) = -\mathbf{H}_\perp(-z)$ of z. On the other hand, the in-plane magnetization of a Néel Sk $\mathbf{n}_\perp \propto \mathbf{k}$. Hence, in this case $\mathbf{H}(z) \neq \mathbf{H}(-z)$ which describes an asymmetry of the magnetic stray field. This asymmetry is a typical feature of stray fields generated by magnetic textures with Néel-like magnetization [32,33].

In order to fully determine the magnetic stray field and the Meissner current, we first need to specify the value of the constant $\mathbf{C}_{\mathbf{r}_\perp}$. Using the condition that the spatial average of the in-plane component of the stray field vanishes, i.e., $\int d\mathbf{r}\mathbf{H}_\perp(\rho, z) = 0$, we get an additional equation for $\mathbf{C}_{\mathbf{r}_\perp}$. For the case of an isolated Sk this constant is equal to zero $\mathbf{C}_{\mathbf{r}_\perp} = 0$. The real-space representation of the screened stray field in Eqs. (20)–(23) can now be easily expressed as

In the S region $|z| > d_F$,

$$\tilde{\mathbf{H}}_\perp^{(S)}(\rho, z) = -\frac{\rho}{\rho}\int_0^\infty dkk J_1(k\rho)\kappa \sinh(kd_F)$$

$$\times \left[\frac{\bar{m}_\perp(k)}{D_2(k)} \mp \frac{m_z(k)}{D_1(k)}\right]e^{-\kappa|z \mp d_F|}, \qquad (37)$$

$$\tilde{H}_z^{(S)}(\rho, z) = -\int_0^\infty dkk J_0(k\rho)k \sinh(kd_F)$$

$$\times \left[\pm\frac{\bar{m}_\perp(k)}{D_2(k)} - \frac{m_z(k)}{D_1(k)}\right]e^{-\kappa|z \mp d_F|}. \qquad (38)$$
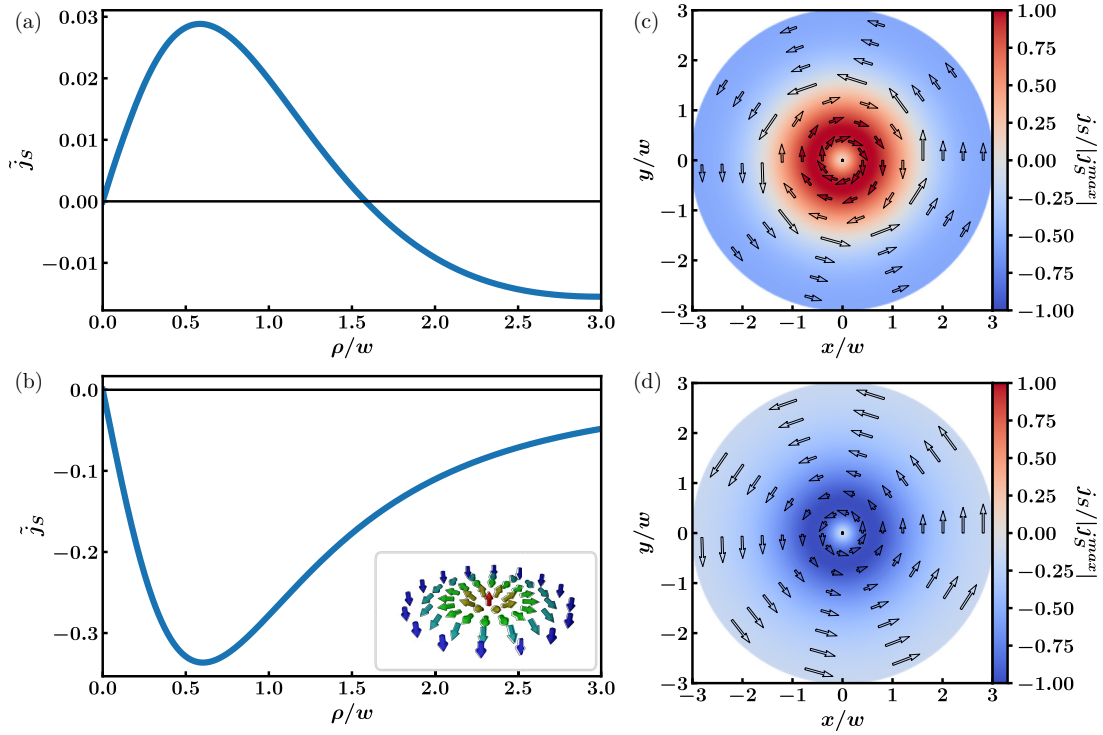
FIG. 1. Radial plots of the normalized Meissner current $\tilde{j}_S = j_S/cM_0\lambda_S^{-2}w$ generated by the stray field of a Néel Sk, shown in the inset of (b), in the (a) upper and (b) lower superconducting regions for $\lambda_L = w$ and $d_F = 10w$. The arrows in the corresponding 2D plots (c) and (d) indicate the direction of the circular screening current. The color map is normalized with respect to the maximal value of j_S in the upper (c) and lower (d) superconductors, respectively. The asymmetry of the stray fields in the upper and lower superconductors leads to a sign change of the Meissner current in the upper S above the Sk region.

In the F film $|z| < d_F$,

$$\tilde{\mathbf{H}}_\perp^{(F)}(\rho, z) = \frac{\rho}{\rho} \int_0^\infty dk k J_1(k\rho)$$

$$\times \left[\bar{m}_\perp(k) \left(\frac{k\cosh(kz)}{D_2(k)} - 1 \right) + m_z(k) \frac{\kappa\sinh(kz)}{D_1(k)} \right], \quad (39)$$

$$\tilde{H}_z^{(F)}(\rho, z) = -\int_0^\infty dk k J_0(k\rho)$$

$$\times \left[\bar{m}_\perp(k) \frac{k\sinh(kz)}{D_2(k)} + m_z(k) \frac{\kappa\cosh(kz)}{D_1(k)} \right] + \frac{1}{2}, \quad (40)$$

where we inserted the magnetization profile Eqs. (28)–(30) and defined

$$\bar{m}_\perp(k) = \begin{cases} m_\perp(k) & \text{Néel Sk} \\ 0 & \text{Bloch Sk} \end{cases}. \quad (41)$$

Analogously, the Meissner current can be found using Eq. (26), which has the following form in real-space

$$\mathbf{j}_S(\rho, z) = cM_0\lambda_L^{-2} \int_0^\infty dk k J_1(k\rho) \sinh(kd_F)$$

$$\times \left[\pm \frac{\bar{m}_\perp(k)}{D_2(k)} - \frac{m_z(k)}{D_1(k)} \right] e^{-\kappa|z \mp d_F|} \hat{\mathbf{e}}_\varphi. \quad (42)$$

The stray field induces circulating supercurrents pointing in $\hat{\mathbf{e}}_\varphi$ direction. Since the supercurrent is linked to the stray field, the Meissner current also features the asymmetry which is related to the magnetization profile of the Néel Sk. Using Eq. (42), this asymmetry can be identified by the changing sign in the term associated with the in-plane contribution of the magnetization. In Fig. 1, we show the spatial dependence of the Meissner current $\mathbf{j}_S(\rho, \pm d_F)$ in the upper (a) and (c) and the lower (b) and (d) superconductors in the presence of a Néel-type Sk in the ferromagnetic material. The curves are displayed for the parameters $\lambda_F = w$ and $d_F = 10w$. As expected, we observe a strong asymmetry in the dependence $\mathbf{j}_S(\rho, d_F)$ and $\mathbf{j}_S(\rho, -d_F)$ in the upper and lower superconductors. The current $\mathbf{j}_S(\rho, d_F)$ in the upper S changes sign at some finite distance within the Sk region whereas the current $\mathbf{j}_S(\rho, -d_F)$ remains negative for all ρ. Note that the sign reversal of the Meissner current in S/F systems has been found earlier [35–37], but its underlying mechanism was different as it was related to the proximity effect. In the case of Bloch Sk, all the mentioned features are missing and the Meissner current in both superconducting regions is the same, see Fig. 2.

IV. FLAT DOMAIN WALLS

In this section, we consider the magnetization profiles of several different periodic flat DW's, as illustrated in Fig. 3. The alignment of magnetization changes across the DW's as
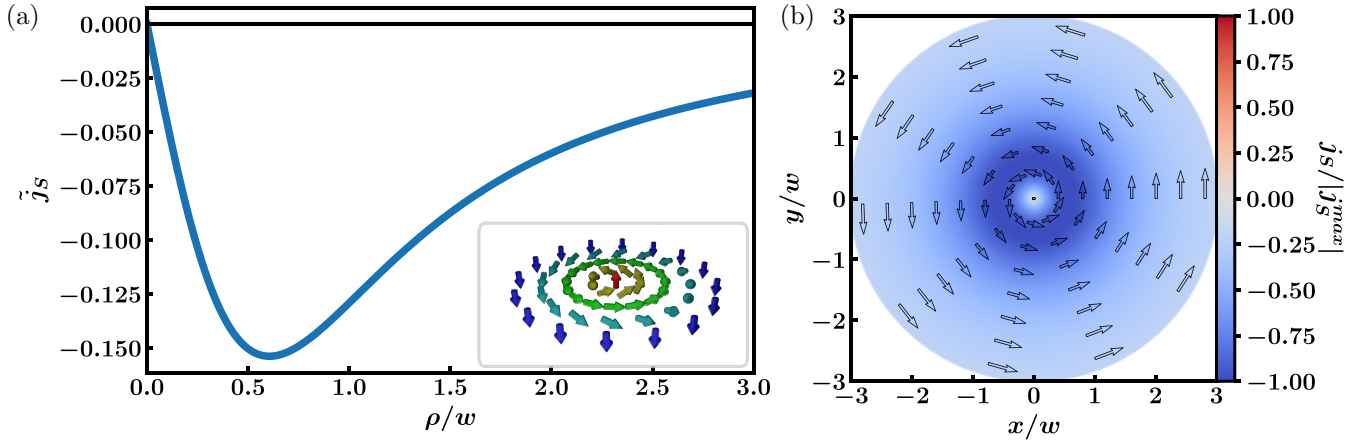
FIG. 2. (a) Radial plots of the normalized Meissner current $\tilde{j}_S = j_S/cM_0\lambda_S^{-2}w$ generated by the stray field of a Bloch Sk (shown in the inset) for $\lambda_L = w$ and $d_F = 10w$. (b) 2D plot of the Meissner current with arrows indicating the direction of the circular screening current. The color map is normalized with respect to the maximal value of j_S. The current is identical for both superconducting regions.

a function of the x coordinate, i.e., $\mathbf{r}_\perp = x\hat{\mathbf{e}}_x$ with $\hat{\mathbf{e}}_x$ being the corresponding unit-vector. The period of the structures is $2L_0$. This enables us to expand all function as a Fourier series: For example, the vector $\mathbf{n}(x,z)$ is represented as

$$\mathbf{n}(x,z) = \sum_{n=-\infty}^{\infty} \mathbf{n}(k_n,z)\exp(ik_nx) \quad (43)$$

with

$$\mathbf{n}(k_n,z) = \frac{1}{2L_0}\int_{-L_0}^{L_0} dx\,\mathbf{n}(x,z)\exp(-ik_nx), \quad (44)$$

where $k_n = \pi n/L_0$. Below we drop the subindex n for brevity.

Now suppose that the vector $\mathbf{n}(x)$ depends only on the x coordinate, i.e., it is completely described by its x component $\mathbf{k} = (k,0)$. In this case, the expression for the normalized magnetic stray field $(\tilde{H}_x(k,z), 0, \tilde{H}_z(k,z))$ and the Meissner current j_S can be obtained in the same manner as in Sec. II. For instance, for two identical S, we obtain the magnetic stray field $\mathbf{H}^{(S)}(k,z)$ by substituting $\mathbf{n}_\perp(k) \to (\mathrm{n}_x(k), 0)$ and $C_{r_\perp} \to (C_x, 0)$ in Eqs. (20) and (21). For periodic DW's, one further needs to replace $\delta(k) \to \sin(kL_0)/kL_0$, which follows from the finite range of integration in Eq. (44). Finally, the

normalized field components in the superconducting regions $|z| > d_F$ are

$$\tilde{H}_x^{(S)}(k,z) = -\kappa\sinh(|k|d_F)\left[\frac{\bar{\mathrm{n}}_x(k)}{D_2(k)} \pm \frac{ik}{|k|}\frac{\mathrm{n}_z(k)}{D_1(k)}\right]e^{-\kappa|z\mp d_F|}, \quad (45)$$

$$\tilde{H}_z^{(S)}(k,z) = -|k|\sinh(|k|d_F)\left[\pm\frac{ik}{|k|}\frac{\bar{\mathrm{n}}_x(k)}{D_2(k)} - \frac{\mathrm{n}_z(k)}{D_1(k)}\right]e^{-\kappa|z\mp d_F|} \quad (46)$$

with

$$\bar{\mathrm{n}}_x(k) := \mathrm{n}_x(k) - C_x\frac{\sin(kL_0)}{kL_0}, \quad (47)$$

and analogously within the ferromagnet $|z| < d_F$,

$$\tilde{H}_x^{(F)}(k,z) = \left[\bar{\mathrm{n}}_x(k)\left(\frac{|k|\cosh(|k|z)}{D_2(k)} - 1\right) - \frac{ik}{|k|}\frac{\mathrm{n}_z(k)\kappa\sinh(|k|z)}{D_1(k)}\right], \quad (48)$$

$$\tilde{H}_z^{(F)}(k,z) = -\left[\frac{ik}{|k|}\frac{\bar{\mathrm{n}}_x(k)|k|\sinh(|k|z)}{D_2(k)} + \frac{\mathrm{n}_z(k)\kappa\cosh(|k|z)}{D_1(k)}\right]. \quad (49)$$

The Meissner current can be extracted from Eq. (26). The supercurrent flows in y direction $\mathbf{j}_S(k,z) = (0, j_S(k,z), 0)$ and has the magnitude

$$j_S(k,z) = cM_0\lambda_L^{-2}\sinh(|k|d_F)\left[\pm\frac{\bar{\mathrm{n}}_x(k)}{D_2(k)} + \frac{ik}{|k|}\frac{\mathrm{n}_z(k)}{D_1(k)}\right]e^{-\kappa|z\mp d_F|}, \quad (50)$$

where once again the $\pm$ indicates the solution in the upper or lower S region, respectively. The current in coordinate representation $\mathbf{j}(x,z)$ can be calculated using

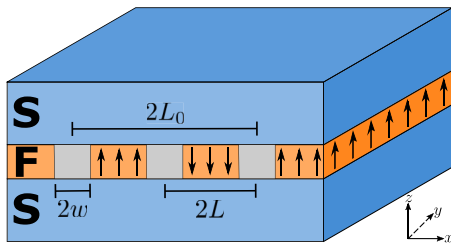$$\mathbf{j}(x,z) = \sum_k \mathbf{j}(k,z)\exp(ikx). \quad (51)$$

FIG. 3. Schematic picture of the S/F/S structure with DW's under consideration. Arrows describe the magnetization vectors $\mathbf{M}$ in the domains with orientation chosen along the z axis. The gray color indicate the domain-wall regions.

Having determined the expressions for $\mathbf{H}_{str}$ and $\mathbf{j}_S$ for an arbitrary type of DW, we need to specify the precise magnetic texture. Its components can be expressed in terms of the
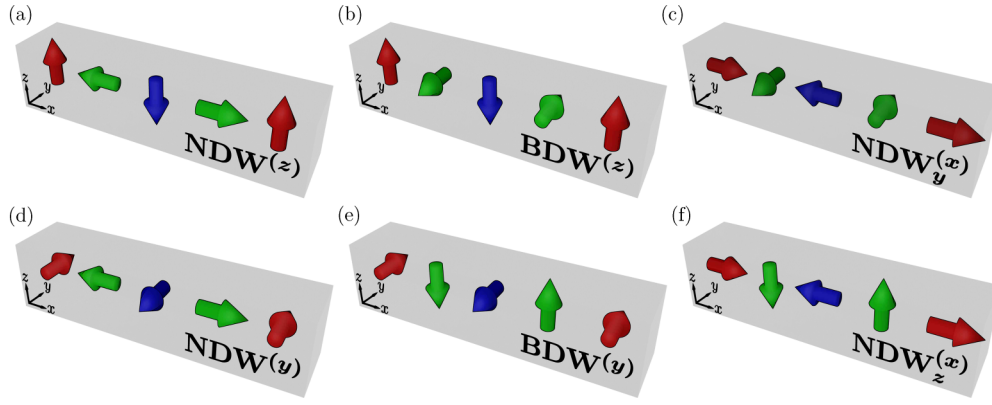
FIG. 4. Schematic representation of a single period of different periodic flat domain wall textures of Néel-type (NDW) and Bloch-type (BDW). The magnetization continuously changes from the domain in the center (blue arrow) to the outer domains (red arrows) via the domain walls (green arrows). The superscripts indicate the orientation of the magnetization across the domain. For orientations along the x direction, there are two possible NDW configuration described by the subscripts y and z. These subscripts describe the axis over which the magnetization changes along the DW.

function n_{even} and n_{odd}, which are characterized by an even or odd dependency on x or k. Since we are interested in a qualitative spatial dependence of all quantities (the fields and the Meisner currents), we approximate $n_{\text{even,odd}}$ by

$$n_{\text{odd}}(x) = \cos\left(\frac{\pi}{2}\frac{(x-L)}{w}\right)\theta(w - |x - L|)$$

$$- \cos\left(\frac{\pi}{2}\frac{(x+L)}{w}\right)\theta(w - |x + L|), \quad (52)$$

$$n_{\text{even}}(x) = \left[1 - \sin\left(\frac{\pi}{2}\frac{(x-L)}{w}\right)\right]\theta(w - |x - L|)$$

$$+ \left[1 + \sin\left(\frac{\pi}{2}\frac{(x+L)}{w}\right)\right]\theta(w - |x + L|)$$

$$+ 2\theta(L - w - |x|) - 1 \quad (53)$$

with the domain wall width $2w$ and the size of the domain $2(L - w)$. That is, we assume that the rotation angle of the vector $\mathbf{n}$ outside the DW's ($|x \mp L| > w$) remains constant whereas it changes linearly inside the DW's ($|x \mp L| < w$). This approximation allows us to present results in a simple analytical form. Outside the interval $|x| < L_0$, $n(x)$ is a periodic function of x: $n(x) = n(x + 2L_0)$. The Fourier components of $n_{\text{odd}}(x)$ and $n_{\text{even}}(x)$ are equal to

$$n_{\text{odd}}(k) = \frac{2\pi i w}{2L_0}\frac{\cos(kw)\sin(kL)}{k^2w^2 - (\pi/2)^2} = \frac{2\pi i w}{2L_0}f(k), \quad (54)$$

$$n_{\text{even}}(k) = \frac{\pi^2}{2L_0 k}\frac{\cos(kw)\sin(kL)}{k^2w^2 - (\pi/2)^2} - \frac{2\sin(kL_0)}{2L_0 k} = \frac{2\pi w}{2L_0}F(k) \quad (55)$$

with

$$f(k) = \frac{\cos(kw)\sin(kL)}{k^2w^2 - (\pi/2)^2}, \quad (56)$$

$$F(k) = \frac{\pi}{2kw}f(k) - \frac{\sin(kL_0)}{\pi kw}. \quad (57)$$

Obviously, $f(k)$ is also an odd function, whereas $F(k)$ is an even function of k. It should be noted that the limiting case of the DW width $w = 0$ was analyzed in Refs. [17,25,26,38].

In our model, the vector $\mathbf{n}$ has two nonzero components that allow the construction of six different magnetic textures (see Fig. 4). They are characterized by vectors $\mathbf{n}$ with the following components: $(0, n_{\text{even}}, n_{\text{odd}})$, $(0, n_{\text{odd}}, n_{\text{even}})$, $(n_{\text{even}}, 0, n_{\text{odd}})$, $(n_{\text{odd}}, 0, n_{\text{even}})$ and $(n_{\text{even}}, n_{\text{odd}}, 0)$, $(n_{\text{odd}}, n_{\text{even}}, 0)$. Note that we are working with the underlying assumption of fixed chirality, i.e., the vector $\mathbf{n}$ rotates in the same direction within the DW's, which is either clockwise or counter-clockwise. Another chirality may be obtained if the rotation of the vector $\mathbf{n}$ in adjacent DW's occurs in different directions; then the function n_{odd} should be replaced by $n_{\text{odd}} \Rightarrow \tilde{n}_{\text{even}}$, where $\tilde{n}_{\text{even}}$ is equal to

$$\tilde{n}_{\text{even}}(x) = \cos\left(\frac{\pi}{2}\frac{(x-L)}{w}\right)\theta(w - |x - L|)$$

$$+ \cos\left(\frac{\pi}{2}\frac{(x+L)}{w}\right)\theta(w - |x + L|), \quad (58)$$

$$\tilde{n}_{\text{even}}(q) = -\frac{2\pi w}{2L_0}\frac{\cos(kw)\cos(kL)}{k^2w^2 - (\pi/2)^2}. \quad (59)$$

In order to obtain our final result for the magnetic stray field and the Meissner current from Eqs. (45)–(50), we need to determine the constant C_x. As mentioned in Sec. II, the average over the in-plane component $H_x^{(\text{F})}$ has to vanish, i.e., $\langle H_x^{(\text{F})}(x, z)\rangle = 0$. From this follows:

$$\langle H_x^{(\text{F})}(x, z)\rangle = \frac{1}{2L_0}\int_{-L_0}^{L_0}dx\frac{1}{2d_{\text{F}}}\int_{-d_{\text{F}}}^{d_{\text{F}}}dz H_x^{(\text{F})}(x, z) \quad (60)$$

$$= \frac{4\pi M_0 \lambda_{\text{L}}^{-1} d_{\text{F}}}{1 + \lambda_{\text{L}}^{-1} d_{\text{F}}}[n_x(k = 0) - C_x] \overset{!}{=} 0, \quad (61)$$

where we used $\int_{-L_0}^{L_0}dx H_x^{(\text{F})}(x, z) = 2L_0 H_x^{(\text{F})}(k = 0, z)$. Hence, the constant C_x is given by
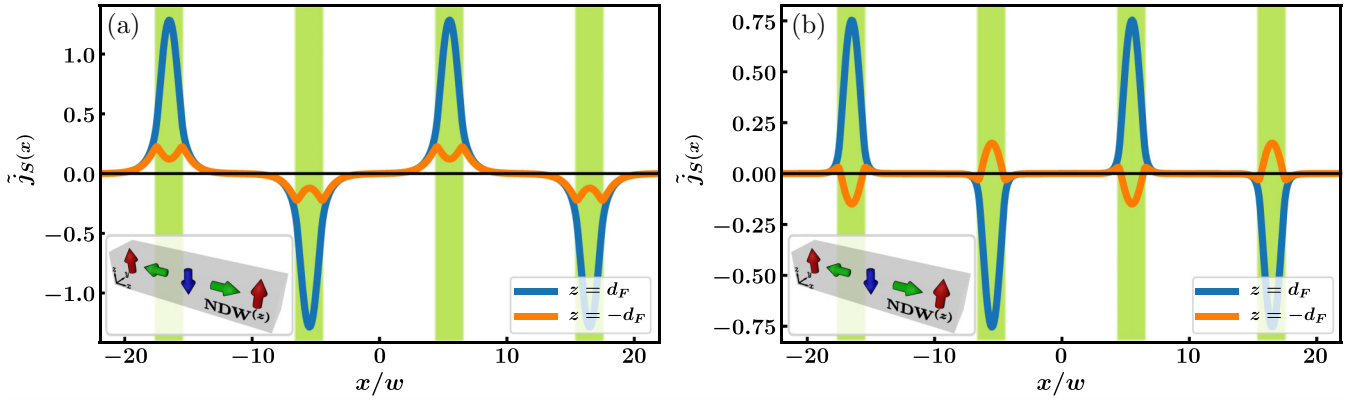
$$C_x = n_x(k = 0, z). \quad (62)$$

FIG. 5. (a) Spatial dependence of the normalized Meissner current $\tilde{j}_S = 2L_0 j_S/(4\pi M_0 c w^2 \lambda_L^{-2})$ for a periodic NDW$^{(z)}$ for $L_0 = 11w$, $L = (11/2)w$, $\lambda_L = w$, and $d_F = 0.2w$. The structure of a single period $2L_0$ of the NDW$^{(z)}$ is shown in the insets. The currents flow mainly above/below the DW regions, which are indicated by the green areas in the figure. The currents above and below the superconductor show a strong asymmetric behavior. (b) Meissner current for the same configuration but with $\lambda_L = (1/3)w$. In this case, the asymmetry can even lead to sign changes across the domain.

The quantity $n_x(k = 0, z)$ can be either $n_{even}(k = 0, z)$ or $n_{odd}(k = 0, z)$. In the latter case, $n_x(k = 0, z) = 0$ [see Eqs. (54) and (56)] and therefore $C_x = 0$. The other case is only realized for certain Néel-type DW's and results in

$$C_x = \frac{2L}{L_0} - 1, \tag{63}$$

i.e., the constant C_x vanishes for $L_0 = 2L$. Otherwise, if $L_0 \neq 2L$, the domains with positive and negative magnetization differ in size, which leads to an uncompensated total magnetization $\mathbf{M}_{un}$ and $C_x \neq 0$. We will now examine the various possible magnetic textures that exhibit a chirality as defined in Eq. (52). Note that the type of DW in a ferromagnetic sample is determined by the existing magnetic interaction and material specific parameters (temperature, thickness of the F film, etc.). Accordingly, the actual magnetic texture in the F corresponds to the configuration associated with the minimum of the thermodynamic potential. Nevertheless, we will find the spatial distribution of the Meissner currents for all possible configurations, bearing in mind that some of these textures might not be energetically favorable, but could be achieved in artificial magnetic structures [33].

A. Out-of-plane n (Néel and Bloch DW's)

For an out-of-plane magnetization, both Néel and/or Bloch DW's [see Figs. 4(a) and 4(b)] can exist within the F. The Néel DW (NDW$^{(z)}$) is described by the following configuration $\mathbf{n}(x)$:

$$\mathbf{n}(x) = (n_{odd}, 0, n_{even}), \quad \text{NDW}^{(z)}. \tag{64}$$

The superscript (z) indicates the alignment of the vector $\mathbf{n}(x)$ across the domains, which is oriented along the z axis. The Meissner current at the interfaces $z = \pm d_F$ is obtain by inserting the corresponding Fourier components in Eq. (50).

$$j_S(k, \pm d_F) = c M_0 \lambda_L^{-2} \sinh(|k|d_F) \frac{2\pi i w}{2L_0}$$
$$\times \left[\pm \frac{f(k)}{D_2(k)} + \frac{\text{sgn}(k)F(k)}{D_1(k)} \right], \tag{65}$$

where $f(k)$ and $F(k)$ are given in Eqs. (56), (57). One can easily see that the current is an odd function of k. In the coordinate representation, we obtain the following result:

$$j_S(x, \pm d_F) = -\frac{4\pi M_0 c w \lambda_L^{-2}}{2L_0} \sum_{k=0}^{\infty} \sin(kx) \sinh(kd_F)$$
$$\times \left[\pm \frac{f(k)}{D_2(k)} + \frac{F(k)}{D_1(k)} \right]. \tag{66}$$

In Fig. 5(a), we plot the dependence of the normalized current $\tilde{j}_S = 2L_0 j_S/(4\pi M_0 c w^2 \lambda_L^{-2})$ for $L_0 = 11w$, $L = (11/2)w$, $\lambda_L = w$ and $d_F = 0.2w$. This plot shows a strong asymmetry between the upper and lower superconductors with currents flowing above/below the DW regions. The direction of the supercurrent depends on the direction of rotation of the DW. Varying the value for the London penetration depth $\lambda_L = (1/3)w$ reveals a sign change for the supercurrent within DW's in the lower supercurrent [see Fig. 5(b)]. One can see that the Meissner currents at different DW's flow in opposite directions. This means that the currents flow along closed loops. Unlike the case of Abrikosov vortices, there is no phase change along these loops. This sign change is similar to the behavior described for the Néel Sk's. As in the case of the Sk, the asymmetry follows from the nonvanishing $\nabla \cdot \mathbf{M}$ term inside the FM, which means that both the bulk and the surface magnetic charges are present. Note that in the zero-width domain wall limit, the n_x component vanishes, i.e., $\nabla \cdot \mathbf{M} = 0$. As a result the asymmetry would disappear.

In the case of a Bloch DW (BDW$^{(z)}$), the vector $\mathbf{n}(x)$ has the components

$$\mathbf{n}(x) = (0, n_{odd}, n_{even}), \quad \text{BDW}^{(z)}, \tag{67}$$

where the magnetization in the domain is once again oriented along the z direction. The Meissner current in Fourier representation is given by

$$j_S(k, \pm d_F) = c M_0 \lambda_L^{-2} \sinh(|k|d_F) \frac{2\pi i w}{2L_0} \frac{\text{sgn}(k)F(k)}{D_1(k)} \tag{68}$$
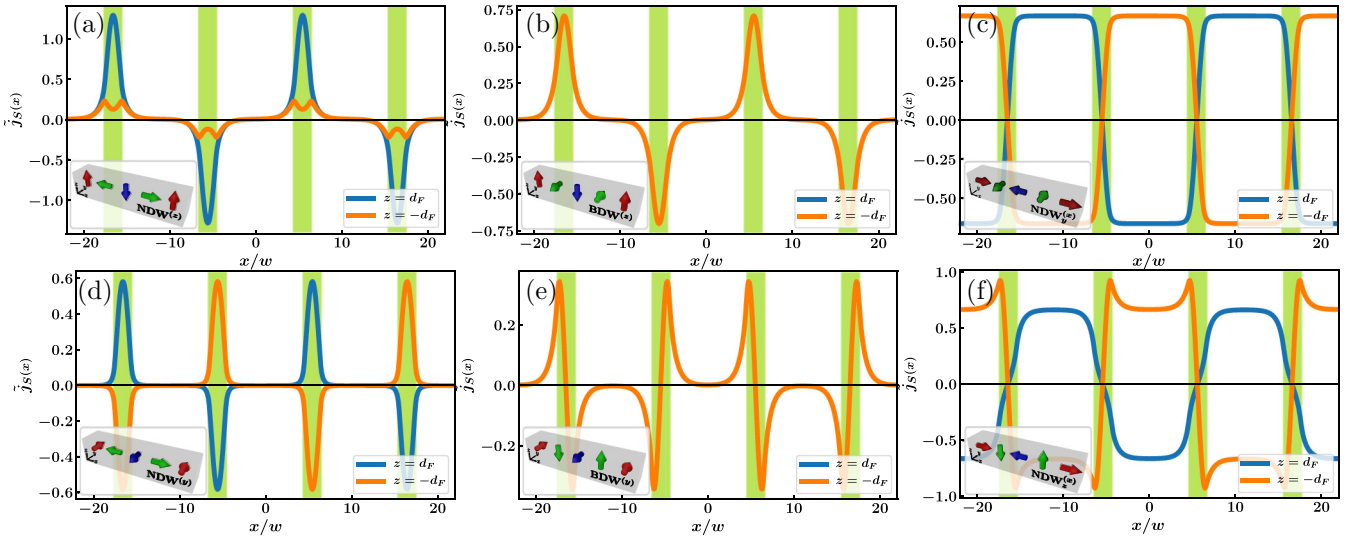
FIG. 6. Spatial dependence of the normalized Meissner current $\tilde{j}_S = 2L_0 j_S / (4\pi M_0 c w^2 \lambda_L^{-2})$ for $L_0 = 11w$, $L = (11/2)w$, $\lambda_L = w$, and $d_F = 0.2w$. The figures describe different periodic magnetic textures (see insets for the depiction of a single period $2L_0$: (a) NDW$^{(z)}$, (b) BDW$^{(z)}$, (c) NDW$_y^{(x)}$, (d) NDW$^{(y)}$, (e) BDW$^{(y)}$, and (f) NDW$_z^{(x)}$). The magnetization continuously changes via the DW's, which are indicated by the green areas. Depending on the underlying magnetization, screening currents preferably flow either above/below the DW [(a), (b), (d) and (e)] or above/below the domain [(c) and (f)]. Their general distribution is unique for every DW structure. In the presence of Bloch-like magnetic textures [(b) and (e)], the Meissner current in the upper and lower superconductors are identical. This is not the case for Neel-like structures, since they exhibit either antisymmetric [(c) and (d)] or even asymmetrical behavior [(a) and (f)].

and in the coordinate representation by

$$j_S(x, \pm d_F) = -\frac{4\pi M_0 c w \lambda_L^{-2}}{2L_0} \sum_{k=0}^{\infty} \sin(kx) \sinh(k d_F) \frac{F(k)}{D_1(k)} \tag{69}$$

One can directly deduce that the resulting Meissner currents are identical in the upper and lower superconductors, which is due to the missing x component of the magnetization. This is once again, similar to the Sk case, as there was also no asymmetry present for Bloch Sk's. For both NDW$^{(z)}$ and BDW$^{(z)}$ follows that $j_S(x, z)$ is an odd function of x so that the total current $J_{av} = \int dx\, j_S(x, \pm d_F)$ vanishes. In Fig. 6(b), we plot the dependence of the Meissner current for the considered case of a BDW$^{(z)}$. The parameter are the same as in Fig. 5.

B. In-plane n (Néel and Bloch DW's)

Let us first consider a Néel-type DW where the magnetization vector $\mathbf{n}(x)$ at the domains is oriented along the y direction [see Fig. 4(d)], then

$$\mathbf{n}(x) = (n_{\text{odd}}, n_{\text{even}}, 0), \quad \text{NDW}^{(y)}. \tag{70}$$

The Fourier component of the Meissner current is equal to

$$j_S(k, \pm d_F) = \pm c M_0 \lambda_L^{-2} \sinh(|k| d_F) \frac{2\pi i w}{2L_0} \frac{f(k)}{D_2(k)} \tag{71}$$

and in the coordinate representation

$$j_S(x, \pm d_F) = \mp \frac{4\pi M_0 c w \lambda_L^{-2}}{2L_0} \sum_{k=0}^{\infty} \sin(kx) \sinh(k d_F) \frac{f(k)}{D_2(k)}. \tag{72}$$

The functions $j_S(x, d_F)$ and $j_S(x, -d_F)$ are shown in Fig. 6(d). Once again the currents differ in the two superconducting

regions. The magnitude of the currents is the same, but the currents flow in opposite direction, resulting in an antisymmetric behavior.

The Bloch type DW [see Fig. 4(e)] is described by

$$\mathbf{n}(x) = (0, n_{\text{even}}, n_{\text{odd}}), \quad \text{BDW}^{(y)}. \tag{73}$$

The occurring currents $j_S(x, z)$ for BDW$^{(y)}$ are even function of x given by

$$j_S(x, \pm d_F) = -\frac{4\pi M_0 c w \lambda_L^{-2}}{2L_0} \sum_{k=0}^{\infty} \cos(kx) \sinh(k d_F) \frac{f(k)}{D_1(k)}. \tag{74}$$

For both $z = \pm d_F$ the currents are equal. In Fig. 6(e), we plot the x dependence of the functions $j_S(x, d_F)$ and $j_S(x, -d_F)$. The Meissner currents in the upper and lower S near the BDW flow in the same direction. The total current j_{av} is zero. The results for $j_S(x, z)$ for the BDW$^{(y)}$ are similiar to those obtained by Burmistrov and Chtchelkatchev [27].

C. Other types of NDW

Other types of NDW's correspond to a magnetization profile $\mathbf{n}(x)$ in which the alignment in the domain is along the x direction [see Figs. 4(c) and 4(f)]. The rotation of the vector $\mathbf{n}(x)$ occurs either in the (x, z) plane or in the (x, y) plane. Thus the vector $\mathbf{n}(x)$ has the components

$$\mathbf{n}(x) = (n_{\text{even}}, n_{\text{odd}}, 0), \quad \text{NDW}_y^{(x)}, \tag{75}$$

$$\mathbf{n}(x) = (n_{\text{even}}, 0, n_{\text{odd}}), \quad \text{NDW}_z^{(x)}. \tag{76}$$

Remember, that for the case $n_x(x) = n_{\text{even}}(x)$ the constant C_x has a finite value given by $C_x = 2L/L_0 - 1$. It follows that

$$\bar{n}_x(k) = n_{\text{even}}(x) - C_x \frac{\sin(kL_0)}{kL_0} = \frac{2\pi w}{2L_0} \bar{F}(k) \quad (77)$$

with

$$\bar{F}(k) = \frac{\pi}{2kw} f(k) - \frac{2L}{L_0} \frac{\sin(kL_0)}{\pi k w}. \quad (78)$$

With this expression, we obtain the Meissner current

$$j_S^1(x, \pm d_F) = \pm \frac{4\pi M_0 c w \lambda_L^{-2}}{2L_0} \sum_{k=0}^{\infty} \cos(kx) \sinh(kd_F) \frac{\bar{F}(k)}{D_2(k)}, \quad (79)$$

$$j_S^2(x, \pm d_F) = \frac{4\pi M_0 c w \lambda_L^{-2}}{2L_0} \sum_{k=0}^{\infty} \cos(kx) \sinh(kd_F)$$

$$\times \left[\pm \frac{\bar{F}(k)}{D_2(k)} - \frac{f(k)}{D_1(k)} \right]. \quad (80)$$

We continue to consider a compensated magnetization where $L_0 = 2L$ so that $\bar{F}(k) = F(k)$.

Once again, we find the typical asymmetry associated with Néel-type magnetic textures. The plots for the two magnetization $\text{NDW}_y^{(x)}$ and $\text{NDW}_z^{(x)}$ can be found in Figs. 6(c) and 6(f), respectively.

V. NUCLEATION OF SUPERCONDUCTIVITY

In this section, we analyze qualitatively the nucleation of superconductivity in S films in an S/F/S structure when the temperature drops below the critical value in a bulk superconductor T_{cB}. The value of the critical temperature T_c differs from its bulk value in the presence of a local depairing factor $V(\mathbf{r}_\perp)$. This problem was analyzed in the case of ferromagnetic superconductors with DW's both theoretically [39–42] and experimentally [40,41,43,44]. Results of intensive studies of hybrid S/F structures are summarized in a review [45]. Theoretical studies were carried out under approximation of zero DW width. In particular the authors of Ref. [42] have studied the so-called diode effect, that is an asymmetrical dependence of the critical current $\mathbf{j}_{cr}$ in the S film with respect to the "magnetic current" $\mathbf{j}_M = \nabla \times \mathbf{M}$. Near the critical temperature at which superconductivity nucleates or disappears, the Ginzburg-Landau equation for the order parameter (OP) ψ can be linearized. In the studies [40–42,46], the OP ψ is presented in the form $\psi = f \exp(i\chi)$, where in a one-dimensional case the phase of the OP is $\chi = kx$. However, in a single-connected superconductor and in the absence of vortices, one can choose a gauge with $\chi = 0$. On the other hand, if we consider our system in the form of a ring (annular geometry) with $x = r\varphi$, then the phase is $\chi = n\varphi$, where φ is the azimuthal angle, n is an integer number of fluxons and R is the radius of the ring. Even in this case, the gauge is not established in a unique way: one can add in principle an arbitrary constant $\mathbf{A}_{\text{ext}}$ to the vector potential $\mathbf{A}$ without changing the observable quantity, the magnetic induction $\mathbf{B} = \nabla \times \mathbf{A}$. From the physical point of view, adding a constant $\mathbf{A}_{\text{ext}}$ means adding a uniform external or spontaneous (in the annular setup) current. Observe that calculating the spatial dependence $A(\mathbf{r}_\perp)$, we assumed, unlike previous theoretical

studies, that $\mathbf{A}_{\text{ext}} = 0$. This means that the total current in the system vanishes $\langle j_S(\mathbf{r}_\perp) \rangle = -(c/4\pi)\langle A(\mathbf{r}_\perp) \rangle = 0$.

Thus, assuming $A_{\text{ext}} = 0$, we consider the Ginzburg-Landau equations for the order parameter f (see, for example, Ref. [41]) near T_c.

$$-d_S \nabla_{\mathbf{r}_\perp}^2 f + V(\mathbf{r}_\perp)f - Ef = -Ef^3, \quad (81)$$

where $V(\mathbf{r}_\perp) = d_S(2\pi\{A_0(\mathbf{r}_\perp) - A_{\text{ext}}\}/\Phi_0)^2$. Here $A_0(\mathbf{r}_\perp)$ is not a gauge invariant quantity, so any observable quantity like the magnetic induction $\mathbf{B} = \nabla \times \mathbf{A}$ will not change by adding a constant A_{ext}. However, in doing so it is necessary to analyze the excitation mechanism of the persistent current and to estimate the condensation energy $E_S = \Delta^2 N(0)V$ in comparison to the magnetic energy $F_I = I_{\text{ext}}^2 \mathcal{L}/c^2$ of the current I_{ext}, where $N(0)$ is the density-of-states in the normal state, $V = 2\pi R(2_S)L_x$ is the volume of the superconductors and $\mathcal{L}$ is the inductance of the superconducting ring. The ratio γ of these two energies depends on various parameters of the system such as the London penetration depth λ_L and the DW width w and may be both smaller or larger than 1. Thus the excitation of the current I_{ext} may not be necessarily energetically favorable. In addition, for a single-connected superconducting system, the problem should be then solved under the condition of the absence of the total current in a finite S/F/S structure disconnected from external circuits. Our solution with $A_{\text{ext}} = 0$ would immediately satisfy these constrains. A more detailed analysis of the problem for a finite current I_{ext} should be left for future studies.

The vector potential A_0 defines the stray field in absence of superconductivity, which can be extracted from Eq. (27) by taking the limit $\lambda_L \to \infty$.

$$\mathbf{A}_0(\mathbf{k}, z) = \frac{4\pi M_0}{|k|} \sinh(|k|d_F)\left(\hat{\mathbf{e}}_z \times \frac{i\mathbf{k}}{|k|}\right)$$

$$\times \left[\pm \frac{i\mathbf{k}}{|k|}\mathbf{n}_\perp(\mathbf{k}) - n_z(\mathbf{k}) \right] e^{-|k||z|}. \quad (82)$$

For simplicity, we assume that the thickness of the S films d_S is smaller than ξ_S, so that the order parameter (OP) f depends only on the in-plane coordinates. At larger d_S, the factor $V(\mathbf{r}_\perp, z)$ depends on the coordinate z and the effect of this depairing factor on the nucleation of superconductivity becomes weaker. Equation (81) is called the time-independent Gross-Pitaevskii [47,48] equation or nonlinear Schrödinger equation. The "energy" E is related to the coherence length $\xi_S(T) = \xi_{S0}/\sqrt{1 - T/T_{cB}}$, $E = d_S/\xi_S^2$. This equation is also used to analyze the nucleation of superconductivity near the critical magnetic field H_{c2} (see Abrikosov's book [49] and [50]) and also near DW in a S/F system [41]. Note also Ref. [51], where this equation is applied for studying the appearance of an OP in a system with two competing OPs.

In the following, we will focus on DW structures where in Eq. (81) $\nabla_{\mathbf{r}_\perp} \to (\partial_x, 0)$. In this case the real space expression for the vector potential at the interface $z = \pm d_F$ is given by

$$\mathbf{A}_0(x, \pm d_F) = -4\pi M_0 \sum_k \frac{\sinh(|k|d_F)}{|k|} e^{ikx}$$

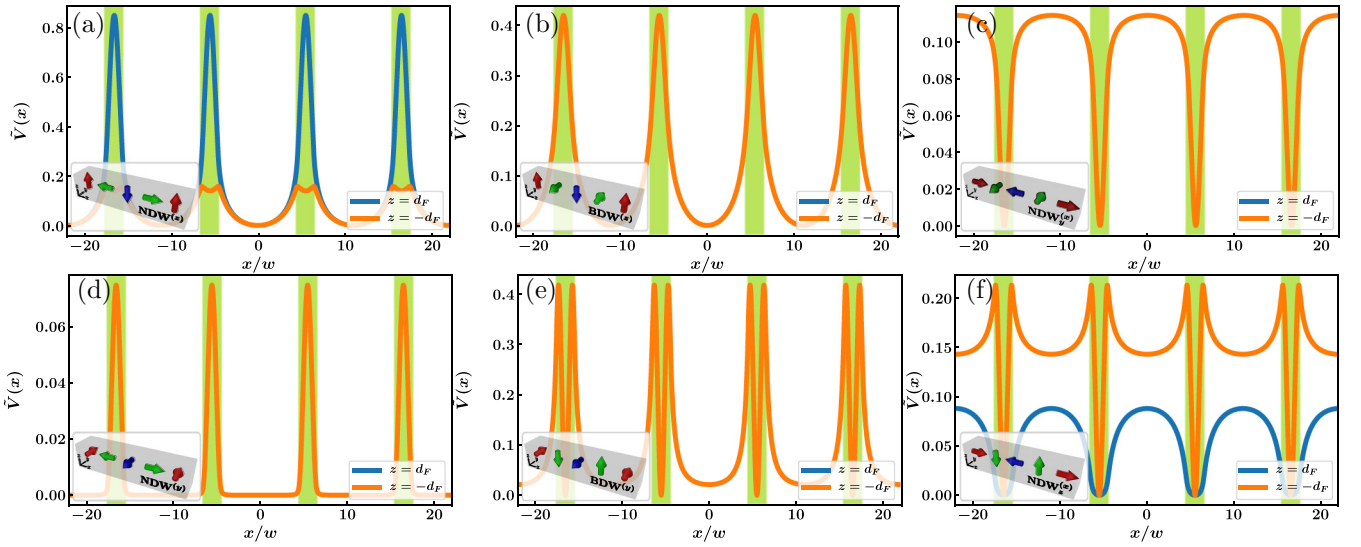$$\times \left[\pm n_x(k) + \frac{ik}{|k|}n_z(k) \right] \hat{\mathbf{e}}_y. \quad (83)$$

FIG. 7. Spatial dependence of the normalized depairing potential $\tilde{V}(x) = d_S V(x)(2L_0\Phi_0/8\pi^2 M_0 w^2)^2$ for $L_0 = 11w$, $L = (11/2)w$, and $d_F = 0.2w$. The figures describe different periodic magnetic textures (see insets for the depiction of a single period $2L_0$: (a) NDW$^{(z)}$, (b) BDW$^{(z)}$, (c) NDW$_y^{(x)}$, (d) NDW$^{(y)}$, (e) BDW$^{(y)}$, and (f) NDW$_x^{(x)}$), where the magnetization continuously changes across the green areas indicating the DW regions. The minima of the potential are either at the DW's [(c), (e), and (f)] or in the center of the domain [(a), (b) and (d)] and correspond to the regions where superconductivity nucleates first. In contrast to the Meissner current (see Fig. 6), there is no antisymmetric behavior for NDW$_y^{(x)}$ (c) and NDW$^{(y)}$ (d), so that the potential in the upper and lower superconductor is the same. In the case of NDW$^{(z)}$ (a) and NDW$_y^{(x)}$ (f), however, the potential remains asymmetric, which should lead to different critical temperatures in the superconductors.

The associated depairing potential $V(x) \propto A_0^2(x)$ is shown in Fig. 7 for the different magnetization configurations. The potential $V(x)$ has minima located either at the DW's ($x = (2n+1)L$, $n = 0, \pm1, \dots$) or in the center of the domains ($x = 2nL$, $n = 0, \pm1, \dots$). The critical temperature T_c is determined by the condition $E_{min} = d_S/\xi_S^2(T_c)$, where E_{min} is the minimal "energy" at which Eq. (81) has a nontrivial solution. We assume that the domain size $2L$ is much larger than the width of the DW $2w$. In the following we consider two possible cases.

A. $V(x)$ has a minimum at the DW

Consider first the case when the potential $V(x)$ has a sharp minimum at the DW, for example, at $\tilde{x} = 0$ where $\tilde{x} = x - L$. Since we are interested in a qualitative picture, we approximate the dependence $V(x)$ near the DW with a rectangular potential well: $V(x) = V_0 - V_0\theta(w - |\tilde{x}|)$. Then, neglecting the right-hand side in Eq. (81) and using the matching conditions at $x = \pm w$ [$f(x)$ and $\partial_x f(x)$ are continuous], we can write a solution in the form

$$f(x) = C_{in}\cos(K_S\tilde{x}), \quad |\tilde{x}| < w, \quad (84)$$

$$f(x) = C_{out}\begin{cases} \exp(-K_{out}(\tilde{x}-w)), & \tilde{x} > w \\ \exp(-K_{out}(\tilde{x}+w)), & \tilde{x} < -w \end{cases}, \quad (85)$$

where $K_S = \xi_S^{-2}(T_c)$ and $K_{out} = (V_0/d_S) - \xi_S^{-2}(T_c)$. The integration constants C_{in} and C_{out} are related to each other. In the limiting cases of small and large $\lambda \equiv \sqrt{V_0 w^2/d_S}$, we have for T_c and C_{in}, C_{out}: (a) $\lambda \ll 1$; $C_{out} \approx C_{in}$ and $T_c \approx T_{cB}(1 - V_0\xi_{S0}^2/d_S)$; and (b) $\lambda \gg 1$; $C_{out} \approx C_{in}/\lambda^2$ and $T_c \approx T_{cB}(1 - (\pi\xi_{S0}/w)^2)$.

Thus, if the depairing potential $V(x)$ has a dip at the DW's, superconductivity is nucleated at the DW's. This happens in the following DW configurations: BDW$^{(y)}$, NDW$_y^{(x)}$, NDW$_z^{(x)}$ (the potentials are shown in Fig. 7). The opposite case is realized for the magnetization profiles: NDW$^{(z)}$, BDW$^{(z)}$, NDW$^{(y)}$ (see also Fig. 7 for the respecting potentials) and is considered in the next section.

For simplicity, we neglect the width w in comparison with L. The solution outside the DW has the form

$$f(x) = C_{out}\cos(K_S x), \quad |x| < L \quad (86)$$

The critical temperature T_c is found from the matching condition $[\partial_x f]_{x=\pm L} = V(x)f(x)|_{x=\pm L}$. The constant $C = C_{out}$ is not zero provided that the condition

$$\theta_c \tan(\theta_c) = \lambda \quad (87)$$

is fulfilled, where $\theta_c = L/\xi_S(T_c)$. Equation (81) yields for the critical temperature T_c: (a) $T_c/T_{cB} = 1 - \lambda(\xi_{S0}/L)^2$ for $\lambda \ll 1$ and (b) $T_c/T_{cB} = 1 - \lambda(\pi\xi_{S0}/2L)^2$ for $\lambda \gg 1$. The constant C is found analogously to the case considered in Ref. [51]

$$C^2 = \frac{T - T_c}{T_{cB} - T_c}r(\theta_L) \quad (88)$$

with

$$r(\theta_L) = \frac{\langle\cos^2(K_S x)\rangle}{\langle\cos^4(K_S x)\rangle}$$
$$= \frac{2\theta_L + \sin(2\theta_L)}{(3/2)\theta_L + \sin(2\theta_L) + (1/8)\sin(4\theta_L)}, \quad (89)$$

where $\langle\dots\rangle = \int_0^L dx(\dots)$ and $\theta_L = K_S L$. For $\theta_L \gg 1$, the coefficient r is equal to $r = 4/3$.

B. $V(x)$ has a minimum at the center of the domain

We assume that the potential $V(x)$ in Eq. (81) has the form

$$V(x) = V_0 \sum_n \delta(x - 2nL). \qquad (90)$$

First, we linearize Eq. (81) and find the minimum "energy" E of the Schrödinger like equation in the interval $x \in -L, L$

$$-\partial_{\tilde{x}\tilde{x}}^2 f + V_0 \delta(\tilde{x}) f(0) = \tilde{E} f, \qquad (91)$$

where $\tilde{x} = x/\xi_{S0}$, $\tilde{E} = E(\xi_{S0}/d_S) = 1 - T/T_{cB}$. A periodic solution $f(\tilde{x}) = f(\tilde{x} + 2L/\xi_{S0})$ can be represented in the form

$$f(\tilde{x}) = \begin{cases} a\cos(q\tilde{x}) + b\sin(q\tilde{x}), & 0 < \tilde{x} < L/\xi_{S0} \\ \bar{a}\cos(q\tilde{x}) + \bar{b}\sin(q\tilde{x}), & -L/\xi_{S0} < \tilde{x} < 0 \end{cases}, \qquad (92)$$

where $q^2 = E$. The function $f(\tilde{x})$ has to fulfill the matching conditions

$$[f] = 0, \quad [\partial_{\tilde{x}} f] = V(\tilde{x})f(0),$$
$$f(L) = f(-L), \quad \partial_{\tilde{x}} f(\tilde{x})|x = L = \partial_{\tilde{x}} f(\tilde{x})|x = -L. \qquad (93)$$

The solution (92) exists if the condition

$$\theta \tan(\theta) = v \equiv VL/2 \qquad (94)$$

is satisfied where $\theta = qL$. The coefficients a and b are coupled by the relations: $a = \bar{a}$, $b = -\bar{b} = Va/2q$. From Eq. (94), we find the critical temperature

$$T_c/T_{cB} = \begin{cases} 1 - (v\xi_{S0}/L)^2, & v \ll 1 \\ 1 - (\pi\xi_{S0}/2L)^2, & v \gg 1 \end{cases}. \qquad (95)$$

If $L/\xi_{S0} > 2/\pi$, superconductivity is suppressed completely.

VI. CONCLUSION

To conclude, in this manuscript we calculated the magnetic stray field $\mathbf{H}_{str}$ and Meissner current $\mathbf{j}_S$ in a superconductors S created by various nonhomogeneous magnetic texture in a F film incorporated in an S/F/S system. The total current in the system is assumed to be zero. Two types of topological structures were considered: isolated chiral magnetic skyrmions and periodic flat domain walls of Bloch (BDW) or Néel-type (NDW). Considering a two-dimensional two-component magnetization $\mathbf{M}(\mathbf{r}_\perp)$, we investigated six different magnetic DW textures as well as magnetic Sk of Bloch and Néel-type. Each of these different magnetic textures possesses a particular spatial dependence of the stray field $\mathbf{H}_{str}(\mathbf{r}_\perp, z)$ and the induced Meissner current $\mathbf{j}_S(\mathbf{r}_\perp, z)$. The most apparent difference appears between the Bloch- and the Néel-type magnetic structures. While the Neel-type structure yields a strong asymmetry $j_S(\mathbf{r}_\perp, z) \neq j_S(\mathbf{r}_\perp, -z)$, the Bloch-type remains always symmetric w.r.t z component. For certain parameter, this asymmetry can be strong enough to cause a sign change of the Meissner current for $\mathbf{r}_\perp$ within the DW region or within the Sk radius $\mathbf{r}_\perp$. Note that a similar sign change can be obtained in S/F or S/F/S systems that feature a proximity effect [35–37].

The Meissner current j_S is connected to the vector potential A via $j_S = c\lambda_L^{-2}A/4\pi$ which enters the Ginzburg-Landau equation and acts as a depairing factor $V(\mathbf{r}_\perp) = 2\pi A_0^2(\mathbf{r}_\perp)$ where A_0 is the vector potential in absence of superconductivity. This factor determines the critical temperature of the superconducting transition in bulk superconductors [49] and in S/F heterostructures [27,41,46] and the superconductivity emerges first at places where A_0 has a minimum. As can be seen in Fig. 7 the locations of the minima or maxima of $V \propto A_0^2$ depends on the type of DW's. For magnetic skyrmions, the depairing potential $V(\mathbf{r}_\perp)$ has its minimum in the center of the Sk. However, it can exhibit an additional local minimum for finite $\mathbf{r}_\perp$ within the radius of a Néel Sk which is not present for Bloch-type skyrmions. Thus, by measuring the location of the superconducting nucleation like it was done previously [31], one can determine the type of the DW or distinguish between Bloch- and Néel-type skyrmions.

[1] A. A. Golubov, M. Y. Kupriyanov, and E. Il'ichev, Rev. Mod. Phys. **76**, 411 (2004).

[2] A. I. Buzdin, Rev. Mod. Phys. **77**, 935 (2005).

[3] F. S. Bergeret, A. F. Volkov, and K. B. Efetov, Rev. Mod. Phys. **77**, 1321 (2005).

[4] M. Eschrig, Rep. Prog. Phys. **78**, 104501 (2015).

[5] J. Linder and J. W. A. Robinson, Nat. Phys. **11**, 307 (2015).

[6] J. Linder and A. Balatsky, Rev. Mod. Phys. **91**, 045005 (2019).

[7] K. Ohnishi, S. Komori, G. Yang, K. R. Jeon, L. A. B. O. Olthof, X. Montiel, M. G. Blamire, and J. W. A. Robinson, Appl. Phys. Lett. **116**, 130501 (2020).

[8] A. A. Abrikosov, Sov. Phys. JETP **5**, 1174 (1957) [Zh. Eksp. Teor. Fiz. **32**, 1442 (1957)].

[9] A. N. Bogdanov and D. Yablonskii, Sov. Phys. JETP **68**, 178 (1989).

[10] A. Leonov, T. Monchesky, N. Romming, A. Kubetzka, A. Bogdanov, and R. Wiesendanger, New J. Phys. **18**, 065003 (2016).

[11] A. Fert, N. Reyren, and V. Cros, Nat. Rev. Mater. **2**, 17031 (2017).

[12] K. Everschor-Sitte, J. Masell, R. M. Reeve, and M. Kläui, J. Appl. Phys. **124**, 240901 (2018).

[13] I. F. Lyuksyutov and V. L. Pokrovsky, Adv. Phys. **54**, 67 (2005).

[14] I. F. Lyuksyutov and V. Pokrovsky, Phys. Rev. Lett. **81**, 2344 (1998).

[15] S. Erdin, I. F. Lyuksyutov, V. L. Pokrovsky, and V. M. Vinokur, Phys. Rev. Lett. **88**, 017001 (2001).

[16] M. V. Milošević and F. M. Peeters, Phys. Rev. B **68**, 094510 (2003).

[17] R. Laiho, E. Lähderanta, E. B. Sonin, and K. B. Traito, Phys. Rev. B **67**, 144522 (2003).

[18] K. M. D. Hals, M. Schecter, and M. S. Rudner, Phys. Rev. Lett. **117**, 017001 (2016).

[19] J. Baumard, J. Cayssol, F. S. Bergeret, and A. Buzdin, Phys. Rev. B **99**, 014511 (2019).

[20] S. M. Dahir, A. F. Volkov, and I. M. Eremin, Phys. Rev. Lett. **122**, 097001 (2019).

[21] R. M. Menezes, J. F. S. Neto, C. Silva, and M. V. Milošević, Phys. Rev. B **100**, 014431 (2019).

[22] S. Rex, I. V. Gornyi, and A. D. Mirlin, Phys. Rev. B **100**, 064504 (2019).

[23] X. Palermo, N. Reyren, S. Mesoraca, A. V. Samokhvalov, S. Collin, F. Godel, A. Sander, K. Bouzehouane, J. Santamaria, V. Cros, A. I. Buzdin, and J. E. Villegas, Phys. Rev. Appl. **13**, 014043 (2020).

[24] L. D. Landau and E. M. Lifshitz, *Electrodynamics of Continuous, Media* (Butterworth-Heinemann, Oxford, 1982).

[25] A. Stankiewicz, S. J. Robinson, G. A. Gehring, and V. V. Tarasenko, J. Phys.: Condens. Matter **9**, 1019 (1997).

[26] L. N. Bulaevskii and E. M. Chudnovsky, Phys. Rev. B **63**, 012502 (2000).

[27] I. S. Burmistrov and N. M. Chtchelkatchev, Phys. Rev. B **72**, 144520 (2005).

[28] A. A. Fraerman, I. R. Karetnikova, I. M. Nefedov, I. A. Shereshevskii, and M. A. Silaev, Phys. Rev. B **71**, 094416 (2005).

[29] G. Yang, P. Stano, J. Klinovaja, and D. Loss, Phys. Rev. B **93**, 224505 (2016).

[30] M. Garnier, A. Mesaros, and P. Simon, Commun. Phys. **2**, 126 (2019).

[31] M. Iavarone, S. A. Moore, J. Fedor, S. T. Ciocys, G. Karapetrov, J. Pearson, V. Novosad, and S. D. Bader, Nat. Commun. **5**, 4766 (2014).

[32] J. Mallinson, IEEE Trans. Magn. **9**, 678 (1973).

[33] M. A. Marioni, M. Penedo, M. Baćani, J. Schwenk, and H. J. Hug, Nano Lett. **18**, 2263 (2018).

[34] N. Romming, A. Kubetzka, C. Hanneken, K. von Bergmann, and R. Wiesendanger, Phys. Rev. Lett. **114**, 177203 (2015).

[35] F. S. Bergeret, A. F. Volkov, and K. B. Efetov, EPL **66**, 111 (2004).

[36] A. F. Volkov, F. S. Bergeret, and K. B. Efetov, Phys. Rev. B **99**, 144506 (2019).

[37] S. Mironov, A. S. Mel'nikov, and A. Buzdin, Appl. Phys. Lett. **113**, 022601 (2018).

[38] E. B. Sonin, Phys. Rev. B **66**, 136501 (2002).

[39] A. I. Buzdin and A. S. Mel'nikov, Phys. Rev. B **67**, 020503(R) (2003).

[40] W. Gillijns, A. Y. Aladyshkin, M. Lange, M. J. Van Bael, and V. V. Moshchalkov, Phys. Rev. Lett. **95**, 227003 (2005).

[41] A. Y. Aladyshkin and V. V. Moshchalkov, Phys. Rev. B **74**, 064503 (2006).

[42] M. A. Silaev, A. Y. Aladyshkin, M. V. Silaeva, and A. S. Aladyshkina, J. Phys.: Condens. Matter **26**, 095702 (2014).

[43] J. Gu, C.-Y. You, J. Jiang, and S. Bader, J. Appl. Phys. **93**, 7696 (2003).

[44] I. C. Moraru, W. P. Pratt, and N. O. Birge, Phys. Rev. Lett. **96**, 037004 (2006).

[45] A. Y. Aladyshkin, A. V. Silhanek, W. Gillijns, and V. V. Moshchalkov, Supercond. Sci. Technol. **22**, 053001 (2009).

[46] A. Y. Aladyshkin, A. I. Buzdin, A. A. Fraerman, A. S. Mel'nikov, D. A. Ryzhov, and A. V. Sokolov, Phys. Rev. B **68**, 184508 (2003).

[47] E. P. Gross, Il Nuovo Cimento (1955-1965) **20**, 454 (1961).

[48] L. P. Pitaevskii, J. Exp. Theor. Phys. (U.S.S.R.) **40**, 646 (1961) [Sov. Phys. JETP **13**, 451 (1961)].

[49] A. A. Abrikosov, *Fundamentals of the Theory of Metals* (North-Holland, Amsterdam, 1988).

[50] A. Abrikosov, J. Exp. Theor. Phys. (U.S.S.R.) **32**, 1442 (1957) [Sov. Phys. JETP **5**, 1174 (1957)].

[51] A. Moor, A. F. Volkov, and K. B. Efetov, Phys. Rev. B **90**, 224512 (2014).